

GPSINDy: Data-Driven Discovery of Equations of Motion

Junette Hsin¹, Shubhankar Agarwal², Adam Thorpe¹, and David Fridovich-Keil¹

Abstract—In this paper, we consider the problem of discovering dynamical system models from noisy data. The presence of noise is known to be a significant problem for symbolic regression algorithms. We combine Gaussian process regression, a nonparametric learning method, with SINDy, a parametric learning approach, to identify nonlinear dynamical systems from data. The key advantages of our proposed approach are its simplicity coupled with the fact that it demonstrates improved robustness properties with noisy data over SINDy. We demonstrate our proposed approach on a Lotka-Volterra model and a unicycle dynamic model in simulation and on an NVIDIA JetRacer system using hardware data. We demonstrate improved performance over SINDy for discovering the system dynamics and predicting future trajectories.

I. INTRODUCTION

An accurate model of dynamics plays a important role in the design and operation of robots. In many cases, it is desirable to obtain analytic expressions over black box models, as analytic models extrapolate well beyond the training dataset and are more suitable for system analysis. One approach that has received significant attention is the Sparse Identification of Nonlinear Dynamics (SINDy) algorithm [1]. It uses symbolic regression—a least-squares-based method—to learn the system dynamics purely from data using a predefined set of candidate functions provided by the user. SINDy is simple in its approach but suffers from several potential drawbacks in practice. In particular, the accuracy of the learned solution relies heavily on the selection of proper candidate function terms, and measurement noise in the data can significantly degrade the performance of SINDy for even simple systems [2]. SINDy also requires derivative data which may be difficult to measure directly and so must be obtained via finite differencing or other approximation methods. Approximation can add additional error, further exacerbating the difficulty of learning the system dynamics [3]. In addition, ordinary least squares does not lead to a sparse representation, and so [1] suggests using either LASSO regression or a sequential optimization procedure called Sequentially Thresholded Least Squares (STLS) where at each step the candidate library is pruned via a thresholding procedure to eliminate the terms that correspond to the smallest coefficients. This can present challenges in the case where noise is present, since some terms can become “lost” in the noise [2]. *In this work, we propose to filter noise using Gaussian process regression to learn the system dynamics purely from data using SINDy.*

The major advantage of SINDy lies in its ability to discover interpretable parametric models while balancing accuracy and parsimony in the learned solution. While other data-driven methods have had success in identifying models from data [4]–[6], insufficient data often limit the effectiveness of such techniques across diverse application areas, and the models they discover do not allow insight into the underlying structure of the system [7]. In contrast, SINDy has been applied across a wide variety of scientific disciplines to understand the underlying structure of physical phenomena [8]–[26]. In the field of robotics, it has been used to learn the dynamics of actuated systems for the purpose of control [27]–[31], such as learning the model of a jet engine prior to applying feedback linearization and sliding mode control [32]. SINDy is promising because it is based on a simple sparse linear regression that is highly extensible and requires comparatively less data than other model learning methods such as neural networks [7].

However, noise remains a problem. A growing body of research based on SINDy seeks to mitigate the impact of noise on identifying the correct system dynamics. Reactive SINDy [33] uses vector-valued functions with SINDy to uncover underlying biological cell structures from noisy data, but the method can only be applied if the data stem from dynamic systems in an equilibrium state. PiDL-SINDy [34] utilizes a physics-informed neural network with sparse regression to learn the system dynamics, and DSINDy [3] and a modified SINDy using automatic differentiation (AD) [35] simultaneously de-noise the data and identify the governing equations. However, PiDL-SINDy [34] and AD-SINDy [35] run into computational bottlenecks and challenges with the structure of their optimization problems. Derivative-based approaches show promise, but DSINDy makes assumptions on the structure of its function library that may not be true in practice. ESINDy [7] proposes a statistical framework to compute the probabilities of candidate functions from an ensemble of models identified from noisy data, but its approach uses an extension of STLS, which may be subject to the same issues as STLS.

Advancements in non-parametric based approaches also tackle the problem of learning governing equations from noisy data. Neural networks have been used to parameterize the state derivatives through a blackbox differential equation solver [36], and Gaussian processes have been used to infer parameters of linear equations from scarce and noisy observations [37] and generate vector fields to learn nonlinear differential equations [38]. Gaussian process regression is particularly effective as an interpolation tool and at reducing the noise in measurement data [5].

¹Departments of Aerospace Engineering & Engineering Mechanics and ²Electrical and Computer Engineering, University of Texas at Austin, {jhsin, somi.agarwal, adam.thorpe, dfk}@utexas.edu

Our main contribution is an application of Gaussian process regression to filter input data for symbolic regression algorithms, which helps to alleviate the issues caused by measurement noise. Our approach exploits the complementary strengths of parametric and non-parametric techniques for model identification by learning the relationship between the state and the time derivatives through Gaussian processes, and then finding the analytic expressions for how the dynamics evolve over time using SINDy. This is especially useful for noisy, real-world data that comes from actual hardware as opposed to simulation data.

We test our method on simulated data as well as measurements collected from hardware experiments. We compare our results against SINDy and a model discovered using a neural network trained on the same data and show improvement over SINDy and the neural network-trained model.

II. PROBLEM FORMULATION

Consider a system characterized by unknown dynamics

$$\dot{\mathbf{x}}(t) = f(\mathbf{x}(t), \mathbf{u}(t)), \quad (1)$$

where $t \in \mathbb{R}$, $\mathbf{x}(t) \in \mathbb{R}^n$ denotes the state of the system at time t , and $\mathbf{u}(t) \in \mathbb{R}^m$ denotes the control input. We presume that $f: \mathbb{R}^n \times \mathbb{R}^m \rightarrow \mathbb{R}^n$ in (1) is unknown, meaning we have no prior knowledge of the system dynamics or its structure. Instead, we assume that we have access to a dataset \mathbf{X} consisting of a sequence of $r \in \mathbb{N}$ state measurements corrupted by noise and control inputs \mathbf{U} taken at discrete times t_1, t_2, \dots, t_r , given by

$$\begin{aligned} \mathbf{X} &= \{\mathbf{x}(t_1) + \epsilon_1, \mathbf{x}(t_2) + \epsilon_2, \dots, \mathbf{x}(t_r) + \epsilon_r\} \\ \mathbf{U} &= \{\mathbf{u}(t_1), \mathbf{u}(t_2), \dots, \mathbf{u}(t_r)\}, \end{aligned} \quad (2)$$

where $\epsilon_i \sim \mathcal{N}(0, \theta_n^2 I)$. We assume that the derivatives of the state with respect to time $\dot{\mathbf{x}}(t) \in \mathbb{R}^n$ corresponding to $\mathbf{x}(t)$ are not directly measurable. Thus, they must be approximated using only the available data, e.g. using (central) finite differencing. Let $\dot{\mathbf{X}}$ be the approximate state derivatives with respect to time of the points in the dataset \mathbf{X} in (2) after applying the corresponding control input in \mathbf{U} , such that $\dot{\mathbf{X}}_i$ is the derivative of \mathbf{X}_i using control input \mathbf{U}_i .

Intuitively, we can view \mathbf{X} and $\dot{\mathbf{X}}$ as matrices in $\mathbb{R}^{r \times n}$ where the i^{th} row \mathbf{X}_i corresponds to the state at time t_i

$$\mathbf{X} = \begin{bmatrix} -\mathbf{X}_1- \\ -\mathbf{X}_2- \\ \vdots \\ -\mathbf{X}_r- \end{bmatrix}, \quad (3)$$

and the i^{th} row $\dot{\mathbf{X}}_i$ is the time derivative of \mathbf{X}_i . Note that because the state measurements \mathbf{X} are corrupted by measurement noise, the approximation of the derivatives of the state with respect to time in $\dot{\mathbf{X}}$ are coarse approximations of the derivative that may be highly inaccurate or exaggerated.

We assume that the dynamics can be described by a linear combination of relatively few elementary function terms

such as polynomials of varying degrees, sinusoidal terms, or exponential functions. For instance,

$$\dot{\mathbf{x}}(t) = \Theta(\mathbf{x}(t), \mathbf{u}(t))^\top \Xi, \quad (4)$$

where $\Theta(\mathbf{x}(t), \mathbf{u}(t)) \in \mathbb{R}^p$ is the candidate function library of elementary basis functions evaluated at the current state $\mathbf{x}(t)$ and control input $\mathbf{u}(t)$ and $\Xi \in \mathbb{R}^{p \times n}$ is a matrix of real-valued coefficients that weight the candidate function terms. For simplicity, using the dataset \mathbf{X} , the applied control inputs \mathbf{U} , and the state derivatives $\dot{\mathbf{X}}$, we can write the relationship between the datasets via

$$\dot{\mathbf{X}} = \Theta(\mathbf{X}, \mathbf{U})^\top \Xi. \quad (5)$$

In practice, (5) does not exactly hold as the data \mathbf{X} is corrupted by noise, and the approximation of $\dot{\mathbf{X}}$ introduces additional error as given by

$$\dot{\mathbf{X}} = \Theta(\mathbf{X}, \mathbf{U})^\top \Xi + \sigma_n \mathbf{Z}, \quad (6)$$

where \mathbf{Z} is a matrix of independent, identically distributed zero-mean Gaussian entries and σ_n is the magnitude of the standard deviation of the noise.

To find Ξ , one can use ordinary least-squares with noisy \mathbf{X} and $\dot{\mathbf{X}}$ to find the model f from (1). However, this approach does not lead to a sparse representation, instead overfitting the model to the data and finding a solution with nonzero elements in every element of Ξ . Sparsity is desirable as the solution is composed of a linear combination of relatively few columns in $\Theta(\mathbf{X}, \mathbf{U})$. In contrast, LASSO [39] has been shown to work well with this type of noisy data, using L_1 regularization to promote sparsity.

Problem 1 (LASSO for Symbolic Regression). *We seek to solve the LASSO problem*

$$\xi_j = \underset{\xi \in \mathbb{R}^p}{\operatorname{argmin}} \|\Theta(\mathbf{X}, \mathbf{U})^\top \xi - \dot{\mathbf{X}}_j\|_2 + \lambda \|\xi\|_1, \quad (7)$$

where the optimization variable $\xi_j \in \mathbb{R}^p$ is the j^{th} column of Ξ from (6), $\dot{\mathbf{X}}_j$ is the j^{th} column of $\dot{\mathbf{X}}$ from (6), and $\lambda > 0$ is the L_1 regularization parameter.

Solving the LASSO problem yields a solution that is more sparse in representation than one found using least-squares. However, as shown in our experiments, using noisy data in (7) leads to the identification of a model that does not accurately capture the system dynamics and does not extrapolate well for prediction. Thus, mitigating the issues caused by noise is essential to identifying the correct dynamics.

III. APPROACH

Various methods exist for de-noising data such as discrete domain wavelet filtering [40], bandpass filtering [40], total variation regularization [41], and neural networks [42]. In this work, we propose to use a smoothing technique based on Gaussian process regression, or Kriging, to alleviate the issues caused by noise in symbolic regression and improve the accuracy of the analytical model.

Like SINDy, Gaussian process regression yields a model for relating input and output data. Unlike SINDy, Gaussian

process regression is *non*-parametric; it models a probability distribution of the data $\dot{\mathbf{X}}$, which from (5), is a function of \mathbf{X} . This distribution is described by a mean function $m(\cdot)$ and covariance kernel function $k(\cdot, \cdot)$, and the negative log-likelihood of the data $\dot{\mathbf{X}}$ is given by

$$-\log p(\dot{\mathbf{X}}) = \frac{1}{2}(\dot{\mathbf{X}} - m(\mathbf{X}))^\top (K + \sigma_n^2 I)^{-1}(\dot{\mathbf{X}} - m(\mathbf{X})) + \frac{1}{2} \log |K| + \frac{n}{2} \log(2\pi), \quad (8)$$

with $K = k(\mathbf{X}, \mathbf{X})$,

where σ_n is a tunable hyperparameter that controls noise variance. The performance of Gaussian process regression also depends heavily on the choice of the kernel. Depending on the chosen kernel, the regression can exhibit notable shortcomings in extrapolation relative to parametric regression. Specifically, the predicted mean can revert to the mean function deduced from the training dataset [5]. In this work, we consider the standard squared-exponential kernel, characterized by its tunable hyperparameters: σ_f (signal variance) and σ_l (length scale)

$$k(\mathbf{X}_i, \mathbf{X}_j) = \sigma_f^2 \exp\left(-\frac{1}{2\sigma_l^2} \|\mathbf{X}_i - \mathbf{X}_j\|^2\right). \quad (9)$$

In practice, the hyperparameters are determined by minimizing (8) with respect to σ_f , σ_l , and σ_n . To use Gaussian process regression as a de-noising tool for the purpose of discovering system dynamics from noisy data, we first assume that $\dot{\mathbf{X}}$ was generated from a Gaussian process at training points \mathbf{X} . Now, let $\dot{\mathbf{X}}_*$ be a random Gaussian vector generated from a Gaussian process at desired test outputs \mathbf{X}_* . We define the joint distribution for $\dot{\mathbf{X}}$ and $\dot{\mathbf{X}}_*$ as

$$\begin{bmatrix} \dot{\mathbf{X}}_* \\ \dot{\mathbf{X}} \end{bmatrix} \sim \mathcal{N}\left(\begin{bmatrix} 0 \\ 0 \end{bmatrix}, \begin{bmatrix} K(\mathbf{X}_*, \mathbf{X}_*) & K(\mathbf{X}_*, \mathbf{X}) \\ K(\mathbf{X}, \mathbf{X}_*) & K(\mathbf{X}, \mathbf{X}) + \sigma_n^2 I \end{bmatrix}\right), \quad (10)$$

where n is the number of training points, and n_* is the number of test points. $K(\mathbf{X}, \mathbf{X}_*)$ denotes the $n \times n_*$ matrix of the covariances evaluated at all pairs of training and test points, $K(\mathbf{X}, \mathbf{X})$ is a $n \times n$ matrix of covariances, and likewise for $K(\mathbf{X}_*, \mathbf{X})$ and $K(\mathbf{X}_*, \mathbf{X}_*)$. To obtain smoothed estimates of $\dot{\mathbf{X}}$ evaluated at the test points, we condition the distribution of the training data on the test data to compute the posterior mean

$$\dot{\mathbf{X}}_{GP} = K(\mathbf{X}_*, \mathbf{X})[K(\mathbf{X}, \mathbf{X}) + \sigma_n^2 I]^{-1} \dot{\mathbf{X}}. \quad (11)$$

Likewise, the joint distribution of the training and test points for the state measurements \mathbf{X} is given by

$$\begin{bmatrix} \mathbf{X}_* \\ \mathbf{X} \end{bmatrix} \sim \mathcal{N}\left(\begin{bmatrix} 0 \\ 0 \end{bmatrix}, \begin{bmatrix} K(\mathbf{t}_*, \mathbf{t}_*) & K(\mathbf{t}_*, \mathbf{t}) \\ K(\mathbf{t}, \mathbf{t}_*) & K(\mathbf{t}, \mathbf{t}) + \theta_n^2 I \end{bmatrix}\right),$$

where $K(\mathbf{t}, \mathbf{t}_*)$ denotes the $n \times n_*$ matrix of the covariances and similarly for $K(\mathbf{t}, \mathbf{t})$, $K(\mathbf{t}_*, \mathbf{t})$ and $K(\mathbf{t}_*, \mathbf{t}_*)$. θ_n is the noise variance hyperparameter for \mathbf{X} . The kernel for \mathbf{X} is characterized by its tunable hyperparameters: θ_f (signal variance) and θ_l (length scale)

$$k(t_i, t_j) = \theta_f^2 \exp\left(-\frac{1}{2\theta_l^2} \|t_i - t_j\|^2\right). \quad (12)$$

To calculate smoothed estimates of \mathbf{X} evaluated at the test points \mathbf{t}_* , we compute the posterior mean

$$\mathbf{X}_{GP} = K(\mathbf{t}_*, \mathbf{t})[K(\mathbf{t}, \mathbf{t}) + \theta_n^2 I]^{-1} \mathbf{X}. \quad (13)$$

Now that we have shown how to obtain \mathbf{X}_{GP} and $\dot{\mathbf{X}}_{GP}$, we move forward to solve the problem in (7).

A. GPSINDy: Symbolic Regression with GP Denoising

First, we minimize the negative log-likelihood of the state \mathbf{X} with respect to the hyperparameters $\theta = [\theta_f, \theta_l, \theta_n]$, assuming its mean function $m(t) = 0$. The negative log-likelihood for \mathbf{X} is given by

$$-\log p(\mathbf{X}) = \frac{1}{2} \mathbf{X}^T (K + \theta_n^2 I)^{-1} \mathbf{X} + \frac{1}{2} \log |K + \theta_n^2 I| + \frac{n}{2} \log(2\pi), \quad (14)$$

with $K = k(\mathbf{t}, \mathbf{t})$.

Then, we condition the distribution of the training data on the test data to obtain the posterior mean of the state evaluated at the test points \mathbf{t}_* according to (13).

Next, we minimize the negative log-likelihood of the state derivative $\dot{\mathbf{X}}$ with respect to the hyperparameters σ_f , σ_l , and σ_n as in (14). Again, we assume a mean function $m(\mathbf{X}) = 0$. Then, we compute the posterior mean $\dot{\mathbf{X}}_{GP}$:

$$\dot{\mathbf{X}}_{GP} = K(\mathbf{X}_{GP*}, \mathbf{X}_{GP})[K(\mathbf{X}_{GP}, \mathbf{X}_{GP}) + \sigma_n^2 I]^{-1} \dot{\mathbf{X}}. \quad (15)$$

Finally, we update the LASSO problem from (7) to use the smoothed states \mathbf{X}_{GP} and derivatives $\dot{\mathbf{X}}_{GP}$ when solving for the coefficients of the system dynamics

$$\xi_j = \underset{\xi \in \mathbb{R}^p}{\operatorname{argmin}} \|\Theta(\mathbf{X}_{GP}, \mathbf{U})^\top \xi - \dot{\mathbf{X}}_{GP,j}\|_2 + \lambda \|\xi\|_1, \quad (16)$$

where $\dot{\mathbf{X}}_{GP,j}$ represents the j^{th} column of $\dot{\mathbf{X}}_{GP}$.

Remark 1 (Distributed Optimization for LASSO). *LASSO can be computationally expensive for large data sets. Fortunately, the objective function in (16) is separable, making it suitable for computational acceleration via splitting methods. One such method, the Alternating Direction Method of Multipliers (ADMM) [43], handles processing of large data sets by splitting its primary variable into two parts and then updating each part in an alternating fashion.*

There is a λ that represents a desirable trade-off between complexity and accuracy, which can be represented by an ‘‘elbow’’ in the Pareto front [44]. To set the sparsity parameter in (16), we can use cross-validation to balance model complexity (determined by the number of nonzero coefficients in Ξ) with accuracy. Cross-validation is used to find the best hyperparameters for a machine learning model by iteratively splitting the data into multiple training and test sets (folds). The model’s performance is evaluated on the test set for different hyperparameter values to find the set that yields the best performance, as shown in [45].

We perform cross-validation with LASSO to achieve a sparse solution with the best model fit based on the dataset. We use ADMM to solve the LASSO problem in (16) to

discover the dynamics for an unknown system using noisy measurements, and we call this method GPSINDy.

IV. EXPERIMENTS & RESULTS

We showcase the efficacy of our proposed approach, GPSINDy, across a spectrum of models: the Lotka-Volterra model for benchmarking, a nonholonomic model (emphasizing unicycle dynamics), and real-world data sourced from the NVIDIA JetRacer system. This latter test underscores GPSINDy’s robustness in handling noisy datasets from real-world hardware. For baselines, we compare our method with the SINDy algorithm [1] and a neural network (NN) based method termed NNSINDy. In the NNSINDy approach, we first refine the noisy data using a NN followed by symbolic regression employing LASSO as detailed in (7). This NN consists of two fully connected layers with 32 hidden neurons and ReLU activations and is trained on the same dataset as GPSINDy using the ADAM optimizer [46]. For all experiments, we refer to the ground-truth coefficients as Ξ_{GT} and the learned coefficients as Ξ_{Learned} .

Experimental Setup: In all of the experiments unless specified, we choose the candidate function library $\Theta(\mathbf{X}, \mathbf{U})$ such that it consists of polynomial terms up to 3rd order, sinusoidal terms (sin and cos), and combinations of the polynomial and sinusoidal terms. For example,

$$\Theta(\mathbf{X}, \mathbf{U}) = \begin{bmatrix} | & | & | & | & | & | \\ 1 & \mathbf{X} & \mathbf{X}^{P_2} & \dots & \sin(\mathbf{U}) & \dots \\ | & | & | & | & | & | \end{bmatrix}, \quad (17)$$

where \mathbf{X}^{P_2} denote higher order polynomials. While we have chosen Θ in this manner for the dynamical systems under consideration in our experiments, it is important to note that in practical applications, the candidate function library $\Theta(\mathbf{X}, \mathbf{U})$ is often broadened to encompass a more diverse set of nonlinear basis functions relevant to the specific system. Additionally, we elect to use LASSO as in (16) in order to maintain consistency and in order to provide a fair point of comparison across all experiments. STLS has been shown to yield better results for noise-free data [2], but in our experiments, this approach failed to yield meaningful results in the presence of noise. For the Gaussian process regression used in experiments, we use the squared exponential kernel and optimize the hyperparameters via maximum likelihood to smooth the measurements.

A. Lotka-Volterra Model (Predator/Prey)

We first consider the problem of identifying the equations of motion for the Lotka-Volterra model [47], which can be used to model the population of predator and prey species over time. The dynamics of the system are given by

$$\dot{x}_1 = ax_1 - bx_1x_2, \quad \dot{x}_2 = -cx_2 + dx_1x_2, \quad (18)$$

where x_1 represents the size of the prey population and x_2 represents the size of the predator population, $a = 1.1$ and $b = 0.4$ describe the prey growth rate and the effect of predation upon the prey population, and $c = 1.0$ and $d = 0.4$

Θ term	Ground Truth		SINDy		GPSINDy	
	\dot{x}_1	\dot{x}_2	\dot{x}_1	\dot{x}_2	\dot{x}_1	\dot{x}_2
x_1	1.1	0.0	1.108	0.0	1.097	0.0
x_2	0.0	-0.1	0.0	-0.997	0.0	-0.980
x_1x_2	-0.4	0.4	-0.397	0.382	-0.358	0.396
x_2x_2	-0.4	0.4	0.0	0.0	0.0	-0.005
$\cos(x_1)$	0.0	0.0	0.0	0.016	-0.049	0.0
$x_1 \cos(x_1)$	0.0	0.0	0.0	-0.005	0.0	0.0
$x_1x_1 \sin(x_2)$	0.0	0.0	-0.003	0.0	0.0	0.0
$x_1x_2 \sin(x_1)$	0.0	0.0	0.0	-0.007	0.0	0.0
$x_1x_2 \sin(x_2)$	0.0	0.0	0.003	0.0	0.0	0.0
$x_1x_1 \cos(x_1)$	0.0	0.0	0.0	-0.009	0.0	-0.003
$x_1x_1 \cos(x_2)$	0.0	0.0	-0.001	0.0	0.0	0.0

TABLE I: **GPSINDy learns better coefficients for the predator-prey model.** In this table we compare the coefficients learned by SINDy and GPSINDy with the ground truth coefficients for the predator-prey model. The bold values show the best learned coefficients compared the the ground-truth coefficients for both \dot{x}_1 and \dot{x}_2 .

describe the predator’s death rate and the growth of predators based on prey population.

We first simulated the system for 30s using the deterministic system dynamics in (18) at discrete time steps $t \in \{t_1, t_2, \dots, t_r\}$ from an initial condition $x_0 = [10, 5]^\top$ with a sampling interval of 0.1s. We collected the deterministic states $\mathbf{x}(t)$ and standardized the data, i.e. normalized to have zero mean and unit variance. In Gaussian process regression, it is common to standardize as scaled data is more useful for hyperparameter optimization. Additionally, the kernel matrix needs to be inverted in (14) and may become ill-conditioned if the data are not properly scaled [48]. We computed the derivatives $\dot{\mathbf{x}}(t)$ from the standardized data using the truth dynamics and then added noise $\epsilon \sim \mathcal{N}(0, \sigma^2)$ on top of the standardized $\mathbf{x}(t)$ and $\dot{\mathbf{x}}(t)$ to simulate measurement noise, thereby obtaining \mathbf{X} and $\dot{\mathbf{X}}$. We set aside the last 20% of the simulated data for validation purposes and used the rest for training. We smoothed \mathbf{X} and $\dot{\mathbf{X}}$ using Gaussian process regression as described in (13) and (11) to obtain \mathbf{X}_{GP} and $\dot{\mathbf{X}}_{GP}$ from the training data and then computed $\Theta(\mathbf{X}_{GP})$ from (17). Finally, using $\dot{\mathbf{X}}_{GP}$ and $\Theta(\mathbf{X}_{GP})$, we solved the L_1 -regularized least-squares problem in (16) using $\lambda = 0.1$. For the baseline NNSINDy, we trained a neural network predict $\dot{\mathbf{X}}$ given the observations of \mathbf{X} using the training data. We performed similar LASSO regression as in GPSINDy to discover the coefficients.

We first compare the learned coefficients Ξ between SINDy and our proposed approach. The coefficients are shown in Table I. We can see that the estimates for the parameters $a, b, c,$ and d obtained by GPSINDy are generally a closer approximation of the true underlying dynamics and that the coefficients matrix Ξ learned by GPSINDy is also more sparse than the one learned by SINDy. As expected, this is because our approach uses Gaussian processes to estimate $\dot{\mathbf{X}}$, which is a smoother approximation of the true derivatives of \mathbf{X} than the one corrupted by noise.

We also quantitatively compare the performance of SINDy, NNSINDy, and GPSINDy on data corrupted by different

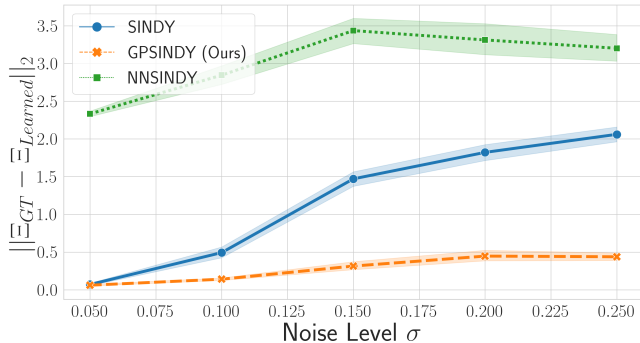


Fig. 1: **GPSINDy outperforms baselines in learning model coefficients for the Predator-Prey model under noisy measurements.** This plot contrasts the coefficients learned by SINDy (blue), GPSINDy (orange), and NNSINDy (green) across varying noise levels for σ , i.e. magnitude of standard deviation. The x-axis represents σ varying from 0.050 to 0.25. The y-axis quantifies the mean-squared error between the ground-truth coefficients (Ξ_{GT}) and the learned coefficients ($\Xi_{Learned}$). Lower overall error is better. Each experiment evaluates coefficients learned from noisy measurements of X and \dot{X} with trials repeated over 40 seeds for each σ .

levels of noise as shown in Figure 1. The results show GPSINDy consistently outperforms the baselines across all noise magnitudes, highlighting its robustness in dealing with noisy data. While SINDy is effective at low noise levels, it struggles at higher levels. NNSINDy, constrained by limited data, fails to effectively learn model coefficients. Furthermore, Figure 2 reveals that trajectories derived from GPSINDy’s learned coefficients align more closely with the ground truth than those of SINDy and NNSINDy. Notably, even though neural networks usually demand vast data volumes, NNSINDy’s trajectory for $x_2(t)$ aligns well initially. However, it eventually deviates for both $x_1(t)$ and $x_2(t)$.

B. Unicycle Dynamics (Simulation)

We now consider the nonholonomic unicycle system. For this experiment, we produced simulation data based on the dynamics of a unicycle system

$$\begin{aligned} \dot{x}_1 &= x_3 \cos(x_4), & \dot{x}_2 &= x_3 \sin(x_4), \\ \dot{x}_3 &= u_1, & \dot{x}_4 &= u_2. \end{aligned} \quad (19)$$

We fix the control input as a function of time, such that $u_1(t) = \sin(t)$ and $u_2(t) = \frac{1}{2} \cos(t)$. The control inputs were chosen to be deterministic functions of time for experiment purposes; in practice, any function can be chosen that perturb the dynamics. As before, we simulated the system for 30s using the deterministic system dynamics and sampled the system at discrete time steps $t \in \{t_1, t_2, \dots, t_r\}$ with a sampling interval of 0.1s from an initial condition $x_0 = [0, 0, 0.5, 0.5]^\top$. Unlike prior setups, we opted not to standardize the states $x(t)$ since the data spread was already apt for Gaussian process regression.

We determined the state derivatives, $\dot{X}(t)$, using the ground truth dynamics. Measurement noise was emulated by

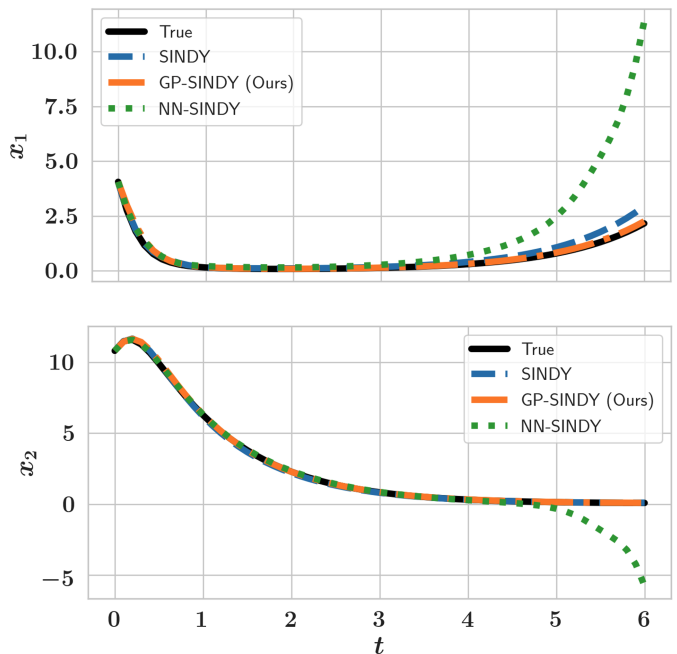


Fig. 2: **Trajectories based on GPSINDy-coefficients closely align with ground truth trajectory for the predator-prey model.** We qualitatively compare the trajectories generated using coefficients learned from SINDy (blue), NNSINDy (green) and GPSINDy (orange) against the ground truth (black) trajectory for the predator-prey model. The coefficients were learned using data with added noise of $\epsilon \sim \mathcal{N}(0, \sigma^2 = 0.05^2)$. The x-axis shows the time and y-axis shows the corresponding states of the predator-prey model. The top figure depicts the x_1 trajectories, while the bottom depicts the x_2 trajectories.

adding Gaussian noise, $\epsilon \sim \mathcal{N}(0, \sigma^2)$, to the true dynamics to obtain X and \dot{X} . As per convention, the last 20% of the simulated data was reserved for validation with the remainder utilized for training. We smoothed X and \dot{X} using (15) and (13) to derive X_{GP} and \dot{X}_{GP} from the training dataset. We then computed the function library $\Theta(X_{GP}, U)$ and finally optimized the L_1 -regularized least-squares problem in (16) with \dot{X}_{GP} and $\Theta(X_{GP}, U)$ using $\lambda = 0.1$ to identify the GPSINDy model. We note that we used polynomial terms up to 1st order in $\Theta(X_{GP}, U)$ as each method failed to identify the truth coefficients when 3rd order terms were included, even when using the deterministic states.

We conduct a quantitative comparison of the performance of SINDy, NNSINDy, and GPSINDy on data affected by various noise levels, as depicted in Figure 3. Notably, GPSINDy consistently outperforms the other methods at higher noise levels, underscoring its resilience against noisy measurements. The performance of NNSINDy and GPSINDy remain relatively consistent between the predator-prey and unicycle systems, but there is a marked degradation in the performance of SINDy for the unicycle system. As the noise levels increase, the efficacy of SINDy diminishes. However, the coefficients learned by all methods in Figure

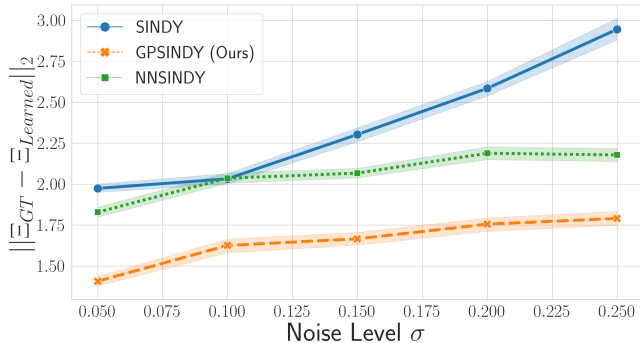


Fig. 3: **GPSINDy outperforms baselines in learning model coefficients for simulated unicycle dynamics under noisy measurements.** This plot contrasts the coefficients learned by SINDy (blue), GPSINDy (orange), and NNSINDy (green) across varying noise levels. The x-axis represents noise level σ varying from 0.05 to 0.25. The y-axis quantifies the mean-squared error between the ground-truth coefficients (Ξ_{GT}) and the learned coefficients ($\Xi_{Learned}$), lower overall error is better. Each experiment evaluates coefficients learned under noisy measurements of \mathbf{X} and $\dot{\mathbf{X}}$, with trials repeated over 40 seeds for each noise level.

3 have relatively large error compared to the results shown in Figure 1, suggesting significant model mismatch with the true unicycle system dynamics. Nevertheless, this experiment demonstrates the ability of GPSINDy to learn more accurate model coefficients even when faced with intricate model dynamics, such as the nonholonomic unicycle system, while using noise-corrupted measurements.

C. JetRacer Hardware Demonstration

We also tested our method real hardware data collected on a NVIDIA JetRacer, a 1/10 scale high speed car. We actuated the car to drive in a figure-8 made up of two circles, 3m in diameter. The nominal time for each lap is 5.5s, resulting in a nominal velocity of 3.4m s^{-1} . VICON sensors captured 22.85s of the system’s motion at discrete timesteps of 0.2s, and the control inputs \mathbf{U} delivered to the robotic system were saved at the same sampling rate. We define the state \mathbf{X}_i at time t_i to be the measured x_1 and x_2 position in m, forward velocity v of the car (with respect to its own frame) in m s^{-1} , and heading angle ϕ (with respect to a global frame) in rad s^{-1} . Each state measurement was then stacked as in (3) to gather \mathbf{X} . Subsequently, we applied central finite differencing to numerically approximate $\dot{\mathbf{X}}$.

As in previous experiments, we split the dataset into a training and testing set. We obtained \mathbf{X}_{GP} and $\dot{\mathbf{X}}_{GP}$ by smoothing \mathbf{X} and $\dot{\mathbf{X}}$ and computed $\Theta(\mathbf{X}_{GP}, \mathbf{U})$. We then solved the L_1 -regularized least squares problem in (16) to obtain the GPSINDy dynamics model. To achieve the best model fit, we tuned λ individually for SINDy and GPSINDy via cross-validation. We started at $\lambda = 1e^{-6}$ and incremented logarithmically until it reached 1. Then, we increased λ in increments of 10 until all of the coefficients were effectively set to 0. We propagated the dynamics for each λ and, at the

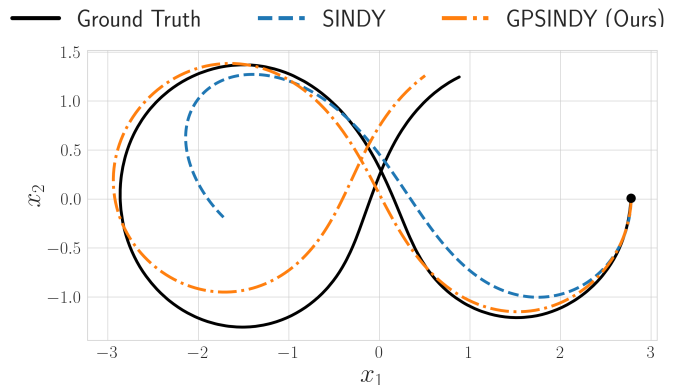


Fig. 4: **GPSINDy Trajectories Align Closely with Ground Truth for the Real JetRacer System.** The plot contrasts trajectories predicted from SINDy (blue) and GPSINDy (orange) with the ground truth (black) based on collected JetRacer data. The axes denote the JetRacer’s Cartesian coordinates. The plot demonstrates that the trajectories derived from GPSINDy-learned coefficients exhibit the closest match to the ground truth while SINDy’s trajectory diverges, reflecting a mismatch between the true JetRacer system dynamics and the model identified by SINDy.

end, selected the λ for each $\dot{\mathbf{X}}$ that fit the data best.

In Figure 4, we compare the performance of the GPSINDy and SINDy-learned dynamics models using the testing dataset from the JetRacer. Both GPSINDy and SINDy capably trace the figure-8 loop navigated by the car. However, the figure shows that GPSINDy, having learned more accurate model coefficients, yields a trajectory that aligns more closely with the ground truth. For the JetRacer run in Figure 4, we juxtapose the trajectories produced by GPSINDy and SINDy against the ground-truth trajectories. **The l_2 error norm between the x and y coordinates for SINDy on the testing data is 1.4m^2 , while for GPSINDy it is reduced to 0.23m^2 .** This outcome underscores GPSINDy’s adeptness at modeling dynamics from noise-afflicted real-world data.

V. CONCLUSIONS & FUTURE WORK

In this paper, we proposed an approach to mitigate the issue of noisy data in sparse symbolic regression algorithms such as SINDy. We used Gaussian process regression to smooth noisy measurements and then used LASSO to achieve sparsity and improved model fit with the data over SINDy. We demonstrated our approach on a Lotka-Volterra system, on an simulated unicycle system, and on noisy data taken from hardware experiments using an NVIDIA JetRacer system. Our results show that a Gaussian process smoothing algorithm significantly improves the task of nonlinear system identification for SINDy. Future work should augment the cost function of SINDy to minimize the log-likelihood while simultaneously learning the nonlinear terms using ADMM, provide a more thorough comparison between existing approaches, and conduct testing on different robotic systems, such as quadrupeds or quadcopters.

REFERENCES

- [1] S. L. Brunton, J. L. Proctor, and J. N. Kutz, "Discovering governing equations from data by sparse identification of nonlinear dynamical systems," *Proceedings of the National Academy of Sciences*, vol. 113, no. 15, pp. 3932–3937, 2016.
- [2] A. Cortiella, K.-C. Park, and A. Doostan, "Sparse identification of nonlinear dynamical systems via reweighted ℓ_1 -regularized least squares," *Computer Methods in Applied Mechanics and Engineering*, vol. 376, p. 113620, 2021.
- [3] J. Wentz and A. Doostan, "Derivative-based SINDy (DSINDy): Addressing the challenge of discovering governing equations from noisy data," *Computer Methods in Applied Mechanics and Engineering*, vol. 413, p. 116096, Aug. 2023. arXiv:2211.05918 [math].
- [4] A. Cochoco and R. Unbehauen, *Neural Networks for Optimization and Signal Processing*. Wiley, 1993.
- [5] C. E. Rasmussen and C. K. Williams, *Gaussian Processes for Machine Learning*. MIT Press, 2006.
- [6] I. Goodfellow, Y. Bengio, and A. Courville, *Deep Learning*. MIT Press, 2016.
- [7] U. Fasel, J. N. Kutz, B. W. Brunton, and S. L. Brunton, "Ensemble-SINDy: Robust sparse model discovery in the low-data, high-noise limit, with active learning and control," *Proceedings of the Royal Society A*, vol. 478, no. 2260, p. 20210904, 2022.
- [8] H. Schaeffer and S. G. McCalla, "Sparse model selection via integral terms," *Physical Review E*, vol. 96, no. 2, p. 023302, 2017.
- [9] A. A. Kaptanoglu, K. D. Morgan, C. J. Hansen, and S. L. Brunton, "Physics-constrained, low-dimensional models for magnetohydrodynamics: First-principles and data-driven approaches," *Physical Review E*, vol. 104, no. 1, p. 015206, 2021.
- [10] K. Kaheman, J. N. Kutz, and S. L. Brunton, "Sindy-pi: a robust algorithm for parallel implicit sparse identification of nonlinear dynamics," *Proceedings of the Royal Society A*, vol. 476, no. 2242, p. 20200279, 2020.
- [11] N. M. Mangan, S. L. Brunton, J. L. Proctor, and J. N. Kutz, "Inferring biological networks by sparse identification of nonlinear dynamics," *IEEE Transactions on Molecular, Biological and Multi-Scale Communications*, vol. 2, no. 1, pp. 52–63, 2016.
- [12] S. Thaler, L. Paehler, and N. A. Adams, "Sparse identification of truncation errors," *Journal of Computational Physics*, vol. 397, p. 108851, 2019.
- [13] L. Boninsegna, F. Nüske, and C. Clementi, "Sparse learning of stochastic dynamical equations," *The Journal of chemical physics*, vol. 148, no. 24, 2018.
- [14] M. Sorokina, S. Sygletos, and S. Turitsyn, "Sparse identification for nonlinear optical communication systems: Sino method," *Optics express*, vol. 24, no. 26, pp. 30433–30443, 2016.
- [15] L. Zanna and T. Bolton, "Data-driven equation discovery of ocean mesoscale closures," *Geophysical Research Letters*, vol. 47, no. 17, 2020.
- [16] M. Schmelzer, R. P. Dwight, and P. Cinnella, "Discovery of algebraic reynolds-stress models using sparse symbolic regression," *Flow, Turbulence and Combustion*, vol. 104, pp. 579–603, 2020.
- [17] S. Beetham, R. O. Fox, and J. Capecealatro, "Sparse identification of multiphase turbulence closures for coupled fluid–particle flows," *Journal of Fluid Mechanics*, vol. 914, p. A11, 2021.
- [18] E. P. Alves and F. Fiuzza, "Data-driven discovery of reduced plasma physics models from fully kinetic simulations," *Physical Review Research*, vol. 4, no. 3, p. 033192, 2022.
- [19] J. L. Callahan, G. Rigas, J.-C. Loiseau, and S. L. Brunton, "An empirical mean-field model of symmetry-breaking in a turbulent wake," *Science Advances*, vol. 8, no. 19, 2022.
- [20] N. Deng, B. R. Noack, M. Morzyński, and L. R. Pastur, "Galerkin force model for transient and post-transient dynamics of the fluidic pinball," *Journal of Fluid Mechanics*, vol. 918, p. A4, 2021.
- [21] Y. Guan, S. L. Brunton, and I. Novosselov, "Sparse nonlinear models of chaotic electroconvection," *Royal Society Open Science*, vol. 8, no. 8, p. 202367, 2021.
- [22] J.-C. Loiseau, "Data-driven modeling of the chaotic thermal convection in an annular thermosiphon," *Theoretical and Computational Fluid Dynamics*, vol. 34, no. 4, pp. 339–365, 2020.
- [23] J.-C. Loiseau, B. R. Noack, and S. L. Brunton, "Sparse reduced-order modelling: sensor-based dynamics to full-state estimation," *Journal of Fluid Mechanics*, vol. 844, pp. 459–490, 2018.
- [24] M. Dam, M. Brøns, J. Juul Rasmussen, V. Naulin, and J. S. Hesthaven, "Sparse identification of a predator-prey system from simulation data of a convection model," *Physics of Plasmas*, vol. 24, no. 2, 2017.
- [25] J.-C. Loiseau and S. L. Brunton, "Constrained sparse galerkin regression," *Journal of Fluid Mechanics*, vol. 838, p. 42–67, 2018.
- [26] M. Sorokina, S. Sygletos, and S. Turitsyn, "Sparse identification for nonlinear optical communication systems: Sino method," *Opt. Express*, vol. 24, no. 26, pp. 30433–30443, 2016.
- [27] F. Abdullah, M. S. Alhajeri, and P. D. Christofides, "Modeling and control of nonlinear processes using sparse identification: Using dropout to handle noisy data," *Industrial & Engineering Chemistry Research*, vol. 61, no. 49, pp. 17976–17992, 2022.
- [28] S. L. Brunton, J. L. Proctor, and J. N. Kutz, "Sparse identification of nonlinear dynamics with control (sindy)," *IFAC-PapersOnLine*, vol. 49, no. 18, pp. 710–715, 2016.
- [29] E. Kaiser, J. N. Kutz, and S. L. Brunton, "Sparse identification of nonlinear dynamics for model predictive control in the low-data limit," *Proceedings of the Royal Society A*, vol. 474, no. 2219, p. 20180335, 2018.
- [30] J. Lore, S. De Pascuale, P. Laiu, B. Russo, J.-S. Park, J. Park, S. Brunton, J. Kutz, and A. Kaptanoglu, "Time-dependent solps-iter simulations of the tokamak plasma boundary for model predictive control using sindy," *Nuclear Fusion*, vol. 63, no. 4, p. 046015, 2023.
- [31] G. Thiele, A. Fey, D. Sommer, and J. Krüger, "System identification of a hysteresis-controlled pump system using sindy," in *2020 24th International Conference on System Theory, Control and Computing (ICSTCC)*, pp. 457–464, IEEE, 2020.
- [32] G. L'Erario, L. Fiorio, G. Nava, F. Bergonti, H. A. O. Mohamed, E. Benenati, S. Traversaro, and D. Pucci, "Modeling, identification and control of model jet engines for jet powered robotics," *IEEE Robotics and Automation Letters*, vol. 5, no. 2, pp. 2070–2077, 2020.
- [33] M. Hoffmann, C. Fröhner, and F. Noé, "Reactive sindy: Discovering governing reactions from concentration data," *The Journal of chemical physics*, vol. 150, no. 2, 2019.
- [34] Z. Chen, Y. Liu, and H. Sun, "Physics-informed learning of governing equations from scarce data," *Nature communications*, vol. 12, no. 1, p. 6136, 2021.
- [35] K. Kaheman, S. L. Brunton, and J. N. Kutz, "Automatic Differentiation to Simultaneously Identify Nonlinear Dynamics and Extract Noise Probability Distributions from Data," Sept. 2020. arXiv:2009.08810 [cs, eess, math].
- [36] R. T. Chen, Y. Rubanova, J. Bettencourt, and D. K. Duvenaud, "Neural ordinary differential equations," *Advances in neural information processing systems*, vol. 31, 2018.
- [37] M. Raissi, P. Perdikaris, and G. E. Karniadakis, "Machine learning of linear differential equations using gaussian processes," *Journal of Computational Physics*, vol. 348, pp. 683–693, 2017.
- [38] M. Heinonen, C. Yildiz, H. Mannerström, J. Intosalmi, and H. Lähdesmäki, "Learning unknown ode models with gaussian processes," in *International conference on machine learning*, pp. 1959–1968, PMLR, 2018.
- [39] R. Tibshirani, *Regression Shrinkage and Selection via the Lasso*. Oxford University Press, 1996.
- [40] S. Bhattacharyya and K. Ghosh, *Noise Filtering for Big Data Analytics*, vol. 12. Walter de Gruyter GmbH & Co KG, 2022.
- [41] P. Rodríguez, "Total variation regularization algorithms for images corrupted with different noise models: a review," *Journal of Electrical and Computer Engineering*, vol. 2013, pp. 10–10, 2013.
- [42] C. Zimmer, M. Meister, and D. Nguyen-Tuong, "Safe active learning for time-series modeling with gaussian processes," in *Advances in Neural Information Processing Systems* (S. Bengio, H. Wallach, H. Larochelle, K. Grauman, N. Cesa-Bianchi, and R. Garnett, eds.), vol. 31, Curran Associates, Inc., 2018.
- [43] S. Boyd, N. Parikh, E. Chu, B. Peleato, and J. Eckstein, "Distributed optimization and statistical learning via the alternating direction method of multipliers," *Foundations and Trends in Machine Learning*, vol. 3, pp. 1–122, 01 2011.
- [44] J. Teich, "Pareto-front exploration with uncertain objectives," in *International Conference on Evolutionary Multi-Criterion Optimization*, pp. 314–328, Springer, 2001.
- [45] K. Ito and R. Nakano, "Optimizing support vector regression hyperparameters based on cross-validation," in *Proceedings of the International Joint Conference on Neural Networks, 2003.*, vol. 3, pp. 2077–2082, IEEE, 2003.

- [46] D. P. Kingma and J. Ba, "Adam: A method for stochastic optimization," *CoRR*, vol. abs/1412.6980, 2015.
- [47] V. Křivan, "Prey–predator models," in *Encyclopedia of Ecology* (S. E. Jørgensen and B. D. Fath, eds.), pp. 2929–2940, Oxford: Academic Press, 2008.
- [48] H. C. Lingmont, F. Alijani, and M. A. Bessa, "Data-driven techniques for finding governing equations of noisy nonlinear dynamical systems," 2020.